Diamondoid Nanostructures as sp 3 -Carbon-Based Gas Sensors

Oana Moncea, Juan Casanova-chafer, Didier Poinsot, Lukas Ochmann, Clève D Mboyi, Houssein Nasrallah, Eduard Llobet, Imen Makni, Molka El atrous, Stéphane Brandès, et al.

Diamondoid Nanostructures as sp^3-Carbon-Based Gas Sensors

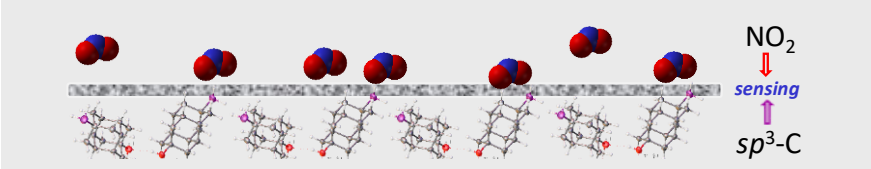

A nanodiamond-based chemical nose: sp^3-C-based diamondoid nanostructures, either Pd-coated or pristine, detect NO_2 and NH_3 at ppb to ppm levels at low operating temperature

O. Moncea, J. Casanova-Chafer, D. Poinsot, L. Ochmann, C. D. Mboyi, H. O. Nasrallah, E. Llobet, I. Makni, M. El Atrous, S. Brandès, Y. Rousselin, B. Domenichini, N. Nuns, A. A. Fokin, P. R. Schreiner,* and J.-C. Hierso**

Diamondoid Nanostructures as sp^3-Carbon-Based Gas Sensors

Diamondoid Nanostructures as sp^3-Carbon-Based Gas Sensors

Oana Moncea,[a,b] Juan Casanova-Chafer,[c] Didier Poinsot,[a] Lukas Ochmann,[b] Clève D. Mboyi,[a] Houssein O. Nasrallah,[a] Eduard Llobet,[c]* Imen Makni,[a] Molka El Atrous,[a] Stéphane Brandès,[a] Yoann Rousselin,[a] Bruno Domenichini,[d] Nicolas Nuns,[e] Andrey A. Fokin,[b,f] Peter R. Schreiner,[b]* and Jean-Cyrille Hierso[a,g]*

Abstract: *Diamondoids, sp^3-hybridized nanometer-sized diamond-like hydrocarbons (nanodiamonds), difunctionalized with hydroxyl and primary phosphine oxide groups enable the assembly of the first sp^3-C-based chemical sensors by vapor deposition. Both pristine nanodiamonds and palladium nanolayered composites can be used to detect toxic NO_2 and NH_3 gases. This carbon-based gas sensor technology allows reversible NO_2 detection down to 50 ppb and NH_3 detection at 25–100 ppm concentration with fast response and recovery processes at 100 °C. Reversible gas adsorption and detection is compatible with 50% humidity conditions. Semiconducting p-type sensing properties are achieved from devices based on primary phosphine-diamantanol, in which high specific area (ca. 140 m^2 g^{-1}) and channel nanoporosity derive from H-bonding.*

Outdoor air pollution, associated with global climate change, causes several million deaths per year.[1] Many toxic gases are produced through combustion processes from vehicles as well as industrial plants. Nitrogen dioxide (NO_2) is the most hazardous gas with a 3 ppm threshold limit value (TLV, human level of exposure to be strictly controlled).[2] NO_2 plays a role in atmospheric reactions causing acid rain, and contributing to ozone formation, which is the major cause of photochemically produced smog.[1,2] Detection and emission control of nitrogen oxides are thus essential objectives to reduce their hazardous effects on environment and mankind.[1-3]

Metal oxide semiconductors are low-cost, robust sensors most frequently used for the NO_2 detection.[4,5] These usually operate at temperatures of a few hundred degrees Celsius, which is costly and reduces sensor lifetime. Other significant limitations are cross-sensitivities with other gases, and detrimental interference from relative humidity. Because of the emergence of nanotechnology a shift in sensor materials occurred toward more sensitive recognition layers,[6] increasingly elaborate architectures,[7,8] and reduced dimensionality.[2,9] Research addresses low-power devices from sensitive and stable sensors usable at moderate temperatures, and thus suited for trace detection for a wide spectrum of applications ranging from lab-on-a-chip and *in vivo* biosensors to environmental monitoring and warfare agent detection.[10] In 2000, the Dai group demonstrated the potential of carbon nanotube (CNT)-based gas sensors.[3] The role of graphene in fabricating gas sensors for the detection of various hazardous gases, including NO_2 rapidly emerged.[11,12] Thus, sensor development experienced a remarkable rise in attention focusing on sp^2-hybridized carbon structures.[13] There is, however, a large group of sp^3-hydridized carbon semiconductor materials, the so-called diamondoids, which essentially are hydrogen-terminated diamond nanoparticles (i.e., pristine nanodiamonds).[14] These mechanically rigid and thermodynamically extremely stable structures[15] are available in large quantities from fossil resources and in part through chemical synthesis.[16] Diamondoids are promising for nanoelectronics,[17] since they exhibit unique effects such as quantum confinement, hence offering possibilities for band gap tuning.[18,19] Diamondoid derivatives serve as building blocks in “bottom-up” strategies to build unique sp^3-carbon-based nanocomposites.[20,21]

Surfaces of CNT-based NO_2 sensor materials react with the detected gas in mechanisms involving charge-transfer or Schottky-barrier modification[2,22] which results in a measurable change in resistance. In semiconducting p-type sensors, electron-donation into the valence band results in charge-carrier recombination causing an increase in resistance. Conversely, electron-withdrawing effects increase the hole concentration in the material, leading to lower resistance.[2] Additionally, NO_2 adsorption is more favorable on CNTs with high metallic character than on semiconducting nanotubes.[23] We thus envisioned that nanocomposites combining sp^3-carbon 3-D molecular-size diamondoids coated with thin metal nanolayers would yield hybrid materials with electronically modified surfaces. These materials would then be potential catalysts or sensors. This band-structure doping inspired approach would combine sp^3-C nanodiamond semiconductors with transition metals. Accordingly, we recently reported robust self-assemblies of volatile P-functionalized diamondoids into nanocrystals via mild vapor deposition,[20] followed by Pd nanolayer coating under mild CVD conditions.[21]

Here we present the first use of sp^3-C-based nanostructures as high sensitivity gas sensors for the reversible detection of NO_2, NH_3, and H_2. These new materials were structurally characterized at different scales (single-crystal X-ray diffraction, powder X-Ray diffraction, porosity measurements, Time-of-Flight Secondary Ion Mass Spectrometry, ToF-SIMS). The materials proved gas responsive both in pristine form and used as metal composite with a thin Pd nanolayer in surface. These chemical p-type sensors promote reversible NO_2 detection at 50 ppb to 100 ppm concentration with fast response and recovery processes at 100 °C; NO_2 detection was even possible in 50% relative humidity. NH_3 detection at 25–100 ppm was also found to be highly efficient.

The primary phosphine 9-(hydroxydiamant-4-yl)phosphine (H_2P–DiamOH, **1**) and its oxide ($H_2(O)P$–DiamOH, **2**) were

[a] Dr. O. Moncea, D. Poinsot, Dr. C. D. Mboyi, Dr. H. O. Nasrallah, I. Makni, M. El Altrous, Dr. Y. Rousselin, Dr. S. Brandès, Prof. Dr. J.-C. Hierso Institut de Chimie Moléculaire de l’Université de Bourgogne (ICMUB) UMR-CNRS 6302, Université de Bourgogne Franche-Comté (UBFC), 9 avenue Alain Savary 21078, Dijon, France
E-mail: jean-cyrille.hierso@u-bourgogne.fr

[b] Dr. O. Moncea, L. Ochmann, Prof. Dr. A. A. Fokin, Prof. Dr. P. R. Schreiner Institute of Organic Chemistry, Justus Liebig University Heinrich-Buff-Ring 17, 35392 Giessen, Germany and Center for Materials Research (LaMa), Justus Liebig University, Heinrich-Buff-Ring 16, 35392 Giessen, Germany
E-mail: prs@uni-giessen.de

[c] J. Casanova-Chafer, Pr. Dr. E. Llobet MINOS-EMaS, University Rovira i Virgili, Avda. Països Catalans, 26, 43007 Tarragona, Spain
E-mail: eduard.llobet@urv.cat

[d] Prof. Dr. B. Domenichini Laboratoire Interdisciplinaire Carnot de Bourgogne (ICB), UMR-CNRS 6303, Université de Bourgogne Franche-Comté (UBFC), 9 avenue Alain Savary 21078, Dijon, France

[e] Dr. N. Nuns Unité de Catalyse et de Chimie du Solide, UMR 8181, Université Lille1 Sciences et Technologies, Cité Scientifique, bâtiment C3 59655, Villeneuve d’Ascq, France

[f] Prof. Dr. A. A. Fokin Department of Organic Chemistry, Kiev Polytechnic Institute Pr. Pobedy 37, 03056 Kiev, Ukraine

synthesized from diamantane (Figures 1 and S1-S2). These diamondoid derivatives were used in powder form, first for their vapor-phase self-assembly, then for generating the metal composites Pd@PH_2–DiamOH (**3**) and Pd@$P(O)H_2$–DiamOH (**4**), respectively.[21] This was achieved by low-temperature chemical vapor deposition of a Pd nanolayer over the crystal self-assembly.[24] We elucidated the structure of **1** by growing single crystals in the vapor phase since all our attempts in solution failed. We found for **1** tetragonal symmetry (space group I-*4*, with a = b = 17.8965(4) Å, c = 8.1224(2) Å, $\alpha = \beta = \gamma = 90°$, V = 2601.48(13) $Å^3$, Tables S1–S4). There is a single molecule in the asymmetric unit with strong H-bonding that leads to tetrameric arrangement (Fig.1).[25] We observed a large-scale arrangement of the crystalline structure in which a significant nanoporosity appears. Channel voids with a total volume of 168 $Å^3$ (~ 6.4% of unit cell, Figure 2) is accessible to small molecules or solvent. We examined voids within related diamondoid structures to establish that cavities in **1** are larger (or exist) than observed for related crystalline diamantane derivatives (see details in Figures S3).

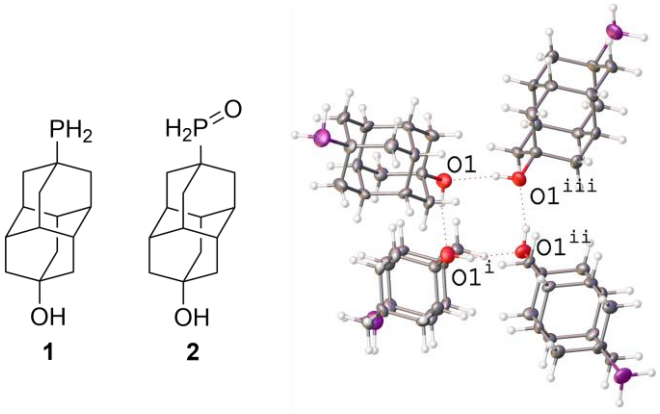

Figure 1. 9-(Hydroxydiamant-4-yl)phosphine 1 and its oxide 2 (left). Tetramer arrangement for 1 with O1–H1•••$O1^{i}$ = 2.737(4) Å and O1–H–$O1^{i}$ = 164.8° (right). Ortep thermal ellipsoids are drawn at 50% probability level.

The powder X-ray diffraction (PXRD) confirmed that this crystalline arrangement is conserved in the granular materials arising from diamantane functionalization, which was used for vapor phase self-assembly of **1** and **2**. We found excellent agreement between the experimental (Figures S4) and simulated PXRD patterns that were obtained from the single crystal unit cell by Le Bail refinement. Two major peaks at *2θ* 15.2° and 15.8°, completed with smaller peaks at 6.9, 9.8, 13.9, and 18.2 ° were observed and calculated. In relation with the XRD channel voids and the highly textured surface observed from SEM (Figure 3, top left), we measured from the crystalline powder the surface area of **1** following the Langmuir method using CO_2 absorption at 198 K (Figures S5a-c). We surprisingly found for this purely organic phosphine a S_{BET} = 138 $m^2\ g^{-1}$, which is significantly higher than several reported porous composite materials.[26] Accordingly, we measured the surface area of the parent diamantyl phosphine (9-hydroxydiamant-4-yl)phosphonic dichloride[15a] (**5**, named Cl_2(O)P–DiamOH) and its chlorinated analogue (9-chlorodiamant-4-yl)phosphonic dichloride (**6**, Cl_2(O)P–Diam–Cl) to found much lower values S_{BET} = 40 and 25 $m^2\ g^{-1}$, respectively (Fig. S5d). While single crystals of **5** could not be obtained, the XRD structure of Cl_2(O)P–DiamCl,[15a] clearly reveals no voids. A S_{BET} = 54 $m^2\ g^{-1}$ was found for the oxide H_2(O)P–DiamOH, **2**.

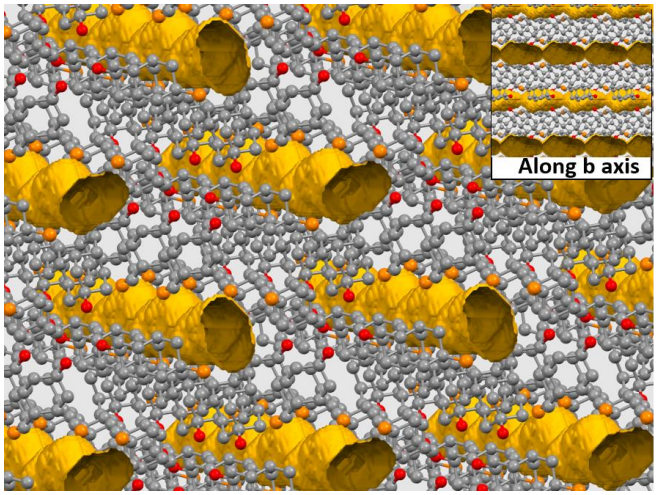

Figure 2. View of accessible channel voids in diamondoid **1** (Platon program crystallographic tool; probe 1.2 Å, grid 0.2 Å).

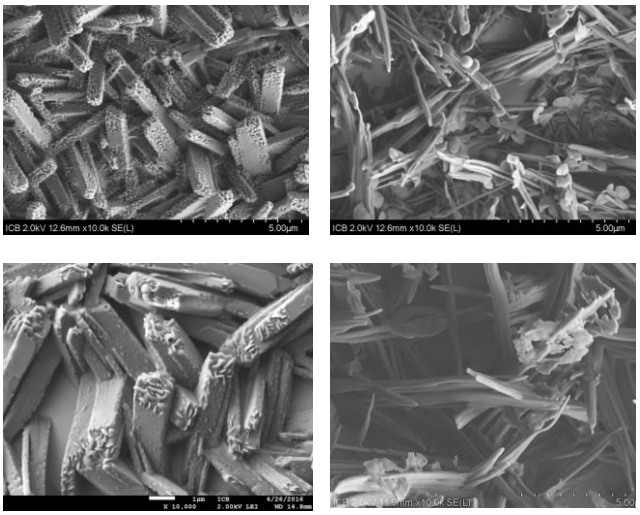

Figure 3. Scanning electron microscopy (SEM) of **1** (top left) and **2** (top right), and metal nanocomposites Pd@PH_2–DiamOH, **3** (bottom left) and Pd@$P(O)H_2$–DiamOH **4** (bottom right).

The nanolayering of palladium over self-assembled **1** and **2** led to nanocomposites **3** and **4**, respectively, for which scanning electron microscopy views are given in Fig. 3. The self-assemblies of **1**-**4** were produced with high structural uniformity and reproducibility.[21] The surfaces composition of these materials has been characterized by XPS, showing covalently built robust Pd@diamondoid hybrids that incorporate Pd–O–$P(H)_n$–diamantane binding motifs. Our initial studies had been limited to a low surface depth below 10 nm, and we thus achieved bulk characterization of these materials in view of gas sensing.

ToF-SIMS analyses (Table S5, Figures S6-S9) from self-assembly of **1** indicated that the surface of primary diamantanol phosphines is mostly in the oxidized form. Additionally, in composite **3** the palladium interactions with oxygen are prevalent, with the palladium isotopic distribution visible in many mass fragments attributable to palladium phosphorus oxides (Table S5, Fig. S6-S9). This is in full agreement with a Pd–O–P bonding scheme suggested by XPS. The ToF-SIMS technique also allowed monitoring and quantifying the different elements of our materials in-depth (bulk) owing to dual beam sputtering and analysis. Figure 4 represents the profile of the elements of interest (Pd, P, C, Si) as a function of sputter time for nanocomposite

Pd@PH_2–DiamOH **3**. The clearly distinguishable areas correspond to the palladium layer (I), diamondoid phosphine deposit (II), and silicon support (III). The steep decrease of curve I from an initially dominant detection attested the Pd present as a thin nanolayer on the surface. The monitoring of phosphorus and carbon from the diamondoid cages (curves II) was achieved through the detection of characteristic fragments (Fig. S6-S9). P and C content detection follow first an increase, while the Pd trace diminishes (the lines cross at 70 s), then they decrease with the emergence of signals from the silicon wafer (curve III, line crossing at 4000 s). The profiles for P-containing and C-containing fragments follow a remarkable parallel evolution that attests to excellent homogeneity of the phosphine diamondoid deposit. According to Yamamura's sputter yield calculation as a function of the sputter type and energy,[27] it is possible to estimate sputter rate for Pd nanolayer (≤ 0.07 nm s^{-1}). ToF-SIMS depth profiling indicates thus a Pd nanolayer thinner than 5 nm. From SEM the diamondoid deposit thickness was estimated above 175 nm.

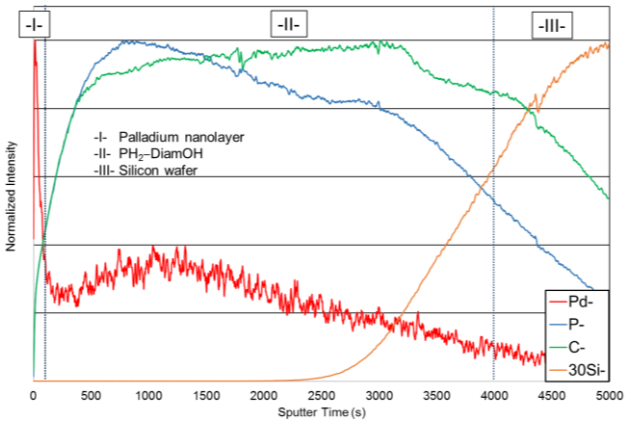

Figure 4. ToF-SIMS depth profile of nanocomposite Pd@PH_2–DiamOH, **3**.

NO_2 gas sensing experiments were conducted with Pd nanocomposites **3** and **4**, but for comparison also with crystal self-assemblies of **1** and **2**. We conducted our experiments in a 35 cm^3 airtight test chamber, with the pieces of silicon wafers glued to a miniaturized ceramic hotplate and connected to a printed circuit board (Figures S10-S11). The exposure to NO_2 was 10 min with a recovery process of 30 min at 100 mL min^{-1} flow of dry air. Nanocomposites operated at 100 °C and their electrical resistance was monitored within repeated response-recovery cycles. The materials were all found responsive (Figure 5). The self-assembly of diamondoid phosphine H_2P–DiamOH **1** showed a NO_2 response (3.0% at 100 ppm, cycling time-resolved detection in Figure 6a) slightly superior to its oxide $H_2(O)P$–DiamOH **2** (1.5% at 100 ppm) and its Pd nanocomposite Pd@PH_2–DiamOH **3** (2.1% at 100 ppm). A significant NO_2 response was achieved with metal nanocomposite Pd@$P(O)H_2$–DiamOH **4** with fast response and recovery processes (4.8% at 100 ppm, cycling detection in Fig. 6b).

The same samples were used for NH_3 detection in the 25–100 ppm concentration range under the same conditions (air flow 100 mL min^{-1}, 100 °C, 35 cm^3 chamber) showing an even higher sensitivity for the NH_3 response (>10.0% for H_2P–DiamOH **1** and >7.0% for Pd@PH_2–DiamOH **3** at 100 ppm NH_3, see cycling time-resolved detection in Fig. 6c and 6d, respectively, and Figure 7a). Exposure to NH_3 (as an electron-donating species) resulted in a resistance increase while the presence of NO_2 (electron-withdrawing) resulted in resistance decrease, which correspond to a typical semiconducting p-type behavior for all samples. Consistently, we found that uptake of H_2 was also possible with nanomaterials **1**–**4**, inducing resistance increase (Figures S12) that confirms the p-type character of these gas sensors. Using the diamondoid phosphine **5** $Cl_2(O)P$–DiamOH,[21] we checked that efficient gas sensing properties were related to the primary phosphine-based diamantanol compounds. We observed for $Cl_2(O)P$–DiamOH-based materials much lower H_2 uptake (if any) compared to **1** (Fig. S12a). This is visibly consistent with the high surface area for gas adsorption in **1** which is found 3.5 time higher than in **5** (138 *vs* 40 m^2 g^{-1}).

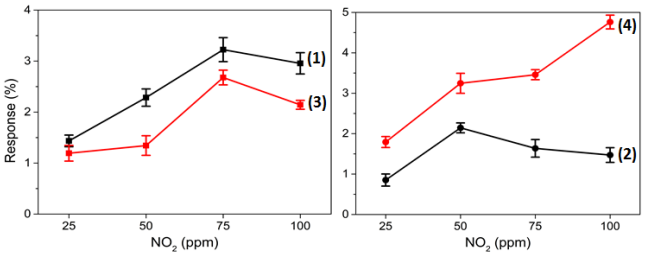

Figure 5. NO_2 response with chemical sensors **1**-**4** at increasing 25 to 100 ppm concentration: ■ = H_2P–DiamOH (**1**), ● = $H_2(O)P$–DiamOH (**2**), ■ = Pd@PH_2–DiamOH (**3**), ● = Pd@$P(O)H_2$–DiamOH (**4**). Response is defined as the relative $(R_{air} - R_{gas})/R_{air}$ after 10 min exposure to NO_2. See also in supporting information (Figures S11).

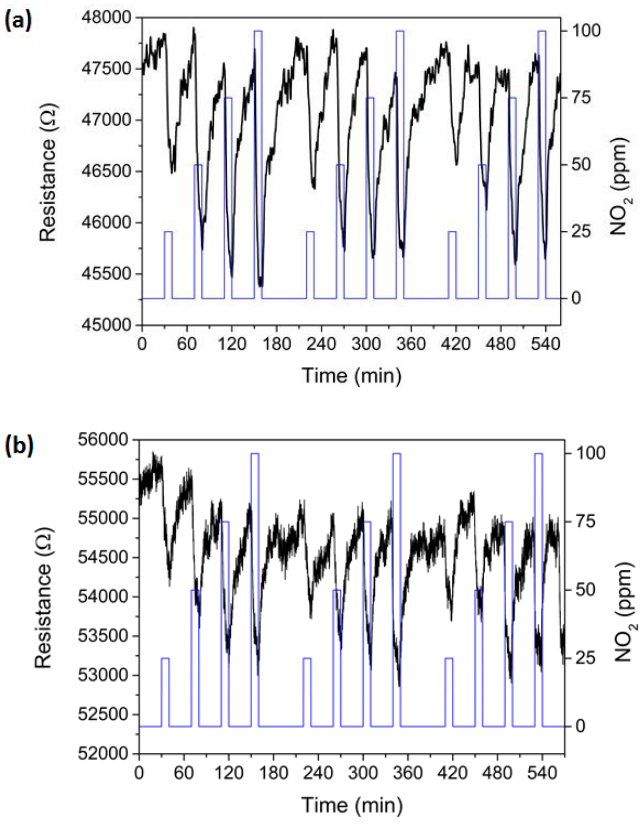

Figure 6a,b. Reversible NO_2 detection for sensors of higher sensitivity at 25, 50, 75, and 100 ppm: H_2P–DiamOH **1** (chart **a**), Pd@$P(O)H_2$–DiamOH **4** (chart **b**). *Signals smoothed using the Savitzky-Golay method*.

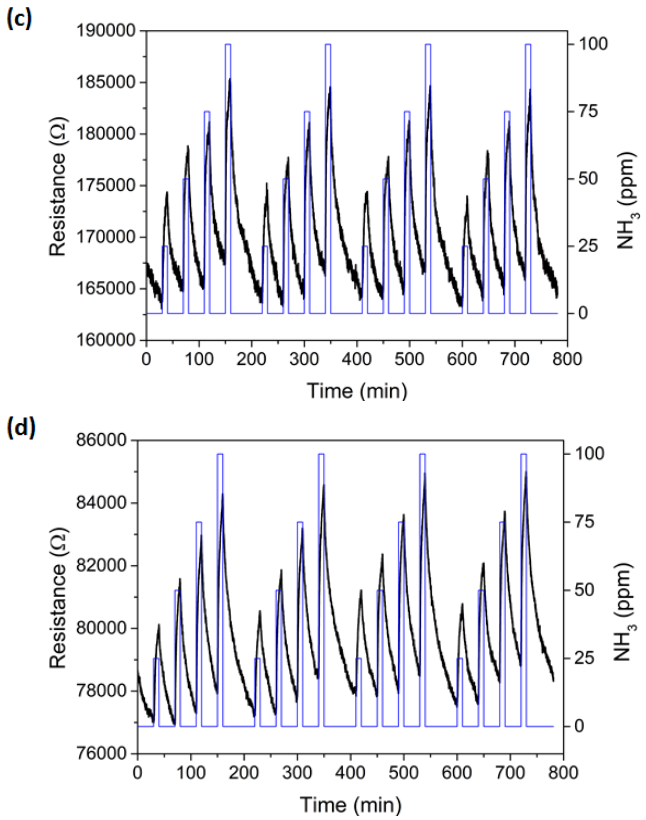

Figure 6c,d. Reversible NH_3 detection for sensors of higher sensitivity at 25, 50, 75, and 100 ppm: H_2P–DiamOH **1** (chart **c**) and Pd@PH_2–DiamOH **3** (chart **d**). *Signals smoothed using the Savitzky-Golay method*.

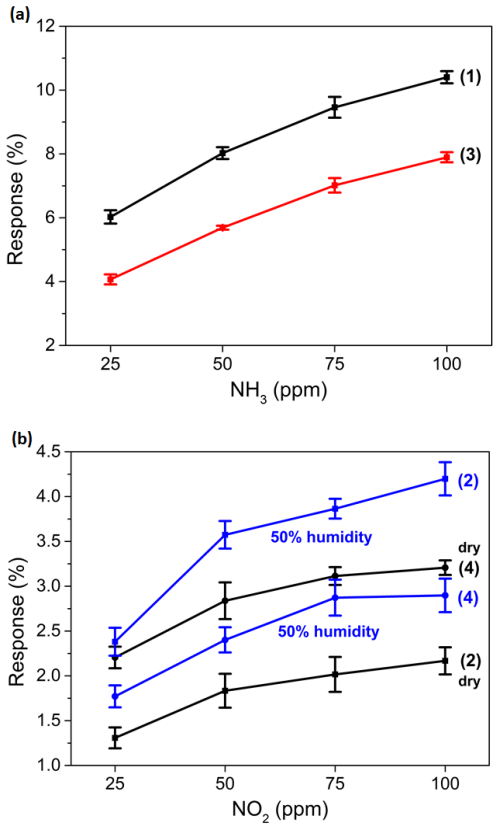

Figure 7. **(a)** NH_3 response of **1** and **3** at increasing 25–100 ppm concentrations (after 10 months storing); **(b)** NO_2 response with sensors **2** and **4** in dry or humid conditions (after six months storing): ■ = $H_2P(O)$–DiamOH (**2**), ● = Pd@$P(O)H_2$–DiamOH (**4**) in dry conditions; ■ = $H_2P(O)$–DiamOH (**2**), ● = Pd@$P(O)H_2$–DiamOH (**4**) in humid conditions (50% relative humidity).

An issue of low-temperature sensing is the potential interference of relative humidity and the sensitivity to water is a factor to consider for practical devices.[2,10] For NO_2 detection we compared the performances of nanomaterials **1**–**4** under dry and humid atmospheres (50% relative humidity) as illustrated in Figure 7b with **4** and **2** (**1** and **3** in Fig. S11.5). The detection of NO_2 was effective under either set of conditions, with different behavior still to rationalize, since **2** (and **3**) increases the sensitivity in humid atmosphere compared to dry conditions, while **4** (and **1**) performed better under dry conditions. In any case the responses were kept detectable in the same range (1–4%). Remarkably, uptake experiments reported in Fig. 7 were achieved six months (NO_2 sensing) to ten months (NH_3 sensing) after device preparation, attesting their robustness upon storing.

Operational devices for toxic gas request a TLV at low level of 25 ppm for NH_3 and 3 ppm for NO_2.[2] While our sp^3-C-based diamondoid sensors efficiently detected NH_3 at this environmental level requirement (Figs. 6 and 7b), we further explored the detection limit of our systems for NO_2 in a 13 cm^3 airtight test chamber, reducing the dead volume with unchanged operating temperature (100 °C) and exposure/recovery times. Under these conditions, the detection of NO_2 concentrations from 50 to 1000 ppb was successfully achieved, and confirmed the suitability of sp^3-carbon-based sensors for detecting few ten ppb of nitrogen dioxide.

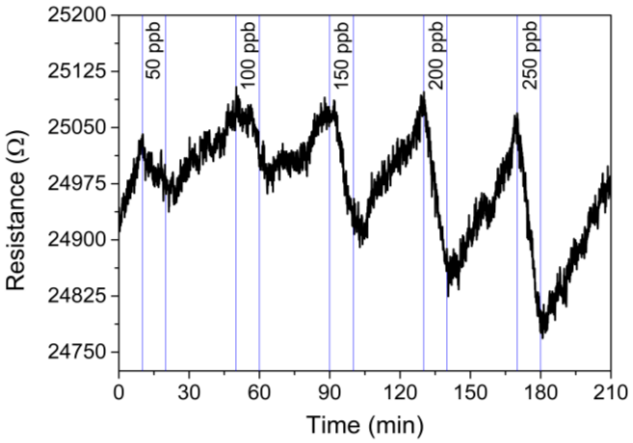

Figure 8. Reversible NO_2 detection at 50–250 ppb level for high sensitivity hybrid nanostructure sensor Pd@PH2–DiamOH **3**.

In summary, we report the first application of sp^3-C-based gas sensors (NO_2, NH_3, and H_2). Remarkably, they tolerate humid conditions and achieve sensing of NO_2 at ppb levels at 100 °C. Pristine and metal-nanolayered diamondoids can both be gas responsive. Such gas sensing properties are related to primary phosphine-diamantanol based compounds for which channel nanoporosity (and S_{Bet} *ca.* 140 m^2 g^{-1}) derives from H-bonding in the solid state. We aim at extending our new approach to other metals and nanoobjects built on suitably functionalized diamondoid sp^3-carbon-based nanostructures.

Acknowledgments

This work was supported by the ANR-DFG program HYBRIDIAMS (ANR-16-CE92-0037-01 and Schr 597/31-1), CNRS, ISITE-BFC, Région BFC and FEDER BFC in 2019. In Tarragona it was supported by MINECO, FEDER (TEC 2015-71663-R) and AGAUR (2017SGR418). EL was supported by the

ICREA Academia Award 2018. The work in Giessen was supported by the U.S. Department of Energy (Contract No. DE-AC02-76SF00515). Mobility was supported by the Université Franco-Allemande/Deutsch-Französische Hochschule. OM, JCC, and DP contributed equally to the work. We thank J.-F. Lamonier, O. Heintz, F. Herbst and R. Chassagnon for their help in the materials characterization.

Keyword: gas sensing • hybrid materials • nanodiamonds • phosphine • palladium •

[1] A. C. Rai, P. Kumar, F. Pilla, A. N. Skouloudis, S. Di Sabatino, C. Ratti, A. Yasar, D. Rickerby, *Sci. Total Environ.* **2017**, *508*, 383 and related World Health Organization (WHO) annual reports cited therein.
[2] D. R. Kauffman, A. Star, *Angew. Chem. Int. Ed.* **2008**, *47*, 6550.
[3] J. Kong, N. R. Franklin, C. Zhou, M. G. Chapline, S. Peng, K. Cho, H. Dai, *Science* **2000**, *287*, 622.
[4] K. Wetchakun, T. Samerjai, N. Tamaekong, C. Liewhiran, C. Siriwong, V. Kruefu, A. Wisitsoraat, A. Tuantranont, S. Phanichphant *Sens. Actuators B* **2011**, *160*, 580.
[5] S. S. Shendage, V. L. Patil, S. A. Vanalakar, S. P. Patil, N. S. Harale, J. L. Bhosale, J. H. Kim, P. S. Patil, *Sens. Actuators B* **2017**, *240*, 426.
[6] M. Schulz, A. Gehl, J. Schlenkrich, H. A. Schulze, S. Zimmermann, A. Schaate *Angew. Chem. Int. Ed.* **2018**, *57*, 12961.
[7] M.-S. Yao, X.-J. Lv, Z.-H. Fu, W.-H. Li, W.-H. Deng, G.-D. Wu, G. Xu, *Angew. Chem. Int. Ed.* **2017**, *56*, 16510.
[8] J. Z. Ou, W. Ge, B. Carey, T. Daeneke, A. Rotbart, W. Shan, Y. Wang, Z. Fu, A. F. Chrimes, W. Wlodarski, S. P. Russo, Y. X. Li, K. Kalantar-zadeh, *ACS Nano* **2015**, *9*, 10313.
[9] a) T. M. Swager, *Angew. Chem. Int. Ed.* **2018**, *57*, 4248. b) G. Cao, Nanostructures and Nanomaterials, Imperial College Press, London, **2004**; c) Z. Chen, J. Appenzeller, J. Knoch, Y. M. Lin, P. Avouris, *Nano Lett.* **2005**, *5*, 1497.
[10] E. Llobet, *Sens. Actuators B* **2013**, *179*, 32.
[11] E. Singh, M. Meyyappan, H. S. Nalwa *ACS Appl. Mater. Interfaces* **2017**, *9*, 34544.
[12] F. Yavari, Z. Chen, A. V. Thomas, W. Ren, H.-M. Cheng, N. Koratkar, *Sci. Rep.* 2011, *1*, 166–1.
[13] V. Schroeder, S. Savagatrup, M. He, S. Lin, T. M. Swager, *Chem. Rev.* **2018**, *118*, DOI: 10.1021/acs.chemrev.8b00340.
[14] a) J. E. Dahl, S. G. Liu, R. M. K. Carlson, *Science* **2003**, *299*, 96; b) H. Schwertfeger, A. A. Fokin, P. R. Schreiner, *Angew. Chem. Int. Ed.* **2008**, *47*, 1022; c) M. A. Gunawan, J.-C. Hierso, D. Poinsot, A. A. Fokin, N. A. Fokina, B. A. Tkachenko, P. R. Schreiner, *New J. Chem.* **2014**, *38*, 28.
[15] a) O. Moncea, M. A. Gunawan, D. Poinsot, H. Cattey, J. Becker, R. I. Yurchenko, E. D. Butova, H. Hausmann, M. Šekutor, A. A. Fokin, J.-C. Hierso, P. R. Schreiner, *J. Org. Chem.* **2016**, *81*, 8759; b) N. A. Fokina, B. A. Tkachenko, A. Merz, M. Serafin, J. E. P. Dahl, R. M. K. Carlson, A. A. Fokin, P. R. Schreiner, *Eur. J. Org. Chem.* **2007**, 4738; c) P.-L. E. Chu, L.-Y. Wang, S. Khatua, A. B. Kolomeisky, S. Link, J. M. Tour, *ACS Nano* **2013**, *7*, 35.
[16] a) J. E. Dahl, J. M. Moldowan, K. E. Peters, G. E. Claypool, M. A. Rooney, G. E. Michael, M. R. Mello, M. L. Kohnen, *Nature* **1999**, *399*, 54; b) J. E. P. Dahl, J. M. Moldowan, T. M. Peakman, J. C. Clardy, E. Lobkovsky, M. M. Olmstead, P. W. May, T. J. Davis, J. W. Steeds, K. E. Peters, A. Pepper, A. Ekuan, R. M. K. Carlson, *Angew. Chem. Int. Ed.* **2003**, *42*, 2040.
[17] a) W. L. Yang, J. D. Fabbri, T. M. Willey, J. R. I. Lee, J. E. Dahl, R. M. K. Carlson, P. R. Schreiner, A. A. Fokin, B. A. Tkachenko, N. A. Fokina, W. Meevasana, N. Mannella, K. Tanaka, X. J. Zhou, T. van Buuren, M. A. Kelly, Z. Hussain, N. A. Melosh, Z.-X. Shen, *Science* **2007**, *316*, 1460; b) W. A. Clay, Z. Liu, W. Yang, J. D. Fabbri, J. E. Dahl, R. M. K. Carlson, Y. Sun, P. R. Schreiner, A. A. Fokin, B. A. Tkachenko, N. A. Fokina, P. A. Pianetta, N. Melosh, Z.-X. Shen, *Nano Lett.* **2009**, *9*, 57; c) Y. Nakanishi, H. Omachi, N. A. Fokina, P. R. Schreiner, R. Kitaura, J. E. P. Dahl, R. M. K. Carlson, H. Shinohara, *Angew. Chem. Int. Ed.* **2015**, *54*, 10802.
[18] G. C. McIntosh, M. Yoon, S. Berber, D. Tománek, *Phys. Rev. B* **2004**, 70, 045401; b) A. A. Fokin, P. R. Schreiner, *Mol. Phys.* **2009**, *107*, 823.
[19] L. Landt, K. Klünder, J. E. Dahl, R. M. K. Carlson, T. Möller, C. Bostedt, *Phys. Rev. Lett.* **2009**, *103*, 047402.
[20] M. A. Gunawan, D. Poinsot, B. Domenichini, C. Dirand, S. Chevalier, A. A. Fokin, P. R. Schreiner, J.-C. Hierso, *Nanoscale* **2015**, *7*, 1956.
[21] M. A. Gunawan, O. Moncea, D. Poinsot, M. Keskes, B. Domenichini, O. Heintz, R. Chassagnon, F. Herbst, J. E. P. Dahl, A. A. Fokin, P. R. Schreiner, J.-C. Hierso, *Adv. Funct. Mater.* **2018**, *28*, 1705786.
[22] Controversy exists over NO_2 uptake mechanisms especially concerning related CNT-based sensors, for a thorough discussion see ref. [2].
[23] a) K. Seo, K. A. Park, C. Kim, S. Han, B. Kim, Y. H. Lee, *J. Am. Chem. Soc.* **2005**, *127*, 15724; b) G. Ruiz-Soria, A. Pérez Paz, M. Sauer, D. J. Mowbray, P. Lacovig, M. Dalmiglio, S. Lizzit, K. Yanagi, A. Rubio, A. Goldoni, P. Ayala, T. Pichler, *ACS Nano* **2014**, *8*, 1375.
[24] a) J.-C. Hierso, C. Satto, R. Feurer, P. Kalck, *Chem. Mater.* **1996**, *8*, 2481; b) J.-C. Hierso, R. Feurer, P. Kalck, *Chem. Mater.* **2000**, *12*, 390.
[25] For 1-D H-bonding network between hydroxylated diamantanes see: Y. Nakanishi, H. Omachi, N. A. Fokina, P. R. Schreiner, J. Becker, J. E. P. Dahl, R. M. K. Carlson, H. Shinohara *Chem. Commun.* **2018**, *54*, 3823.
[26] H. Nasrallah, J.-C. Hierso, *Chem. Mater.* **2019**, *31*, 619.
[27] Y. Yamamura, H. Tawara, *Atomic Data and Nuclear Data Tables*, **1996**, *62*, 149